Preclinical Characterization of AEG35156/GEM 640, a Second-Generation Antisense Oligonucleotide Targeting X-Linked Inhibitor of Apoptosis

Eric C. LaCasse,[1] Gabriele G. Cherton-Horvat,[1] Kimberley E. Hewitt,[1] Lori J. Jerome,[1] Stephen J. Morris,[1] Ekambar R. Kandimalla,[2] Dong Yu,[2] Hui Wang,[3] Wei Wang,[3] Ruiwen Zhang,[3] Sudhir Agrawal,[2] John W. Gillard,[1] and Jon P. Durkin[1]

Abstract

Purpose: Cancer cells can use X-linked inhibitor of apoptosis (XIAP) to evade apoptotic cues, including chemotherapy. The antitumor potential of AEG35156, a novel second-generation antisense oligonucleotide directed toward XIAP, was assessed in human cancer models when given as a single agent and in combination with clinically relevant chemotherapeutics.

Experimental Design: AEG35156 was characterized for its ability to cause dose-dependent reductions of XIAP mRNA and protein *in vitro* and *in vivo*, to sensitize cancer cell lines to death stimuli, and to exhibit antitumor activity in multiple human cancer xenograft models as a single agent or in combination with chemotherapy.

Results: AEG35156 reduced XIAP mRNA levels with an EC_{50} of 8 to 32 nmol/L and decreased XIAP protein levels by >80%. Loss of XIAP protein correlated with increased sensitization to tumor necrosis factor–related apoptosis-inducing ligand (TRAIL)–mediated apoptosis in Panc-1 pancreatic carcinoma cells. AEG35156 exhibited potent antitumor activity relative to control oligonucleotides in three human cancer xenograft models (prostate, colon, and lung) and was capable of inducing complete tumor regression when combined with taxanes. Antitumor effects of AEG35156 correlated with suppression of tumor XIAP levels.

Conclusions: AEG35156 reduces XIAP levels and sensitizes tumors to chemotherapy. AEG35156 is presently under clinical assessment in multiple phase I trials in cancer patients as a single agent and in combination with docetaxel in solid tumors or cytarabine/idarubicin in leukemia.

Chemotherapy is the mainstay of clinical treatment for many solid tumors. However, the development of chemoresistance is a common feature, resulting in a decrease or loss of therapeutic effectiveness. One of the major mechanisms responsible for chemoresistance is the loss of apoptotic sensitivity in cancer cells. Possible causes include alterations in the initiation or execution of the apoptotic machinery, which results from increased activity of antiapoptotic proteins. Novel anticancer therapies that specifically target antiapoptotic mechanisms or that act to lower the apoptotic threshold of cancer cells are in preclinical development or under clinical evaluation (1). An appealing therapeutic candidate target is the X-linked inhibitor of apoptosis (XIAP), a potent antiapoptotic protein whose overexpression and dysfunction is associated with resistance to chemotherapy and radiotherapy (2–5).

Although apoptotic pathways in cells are complex, most seem to converge on a single family of proteases, the caspases that dismantle the cell in an orderly, noninflammatory fashion. The human IAP family, characterized by the presence of one to three baculovirus IAP repeat motifs at the NH_2 terminus of the polypeptide chain (reviewed in refs. 3, 6), are the only known cellular inhibitors of caspases. Specifically, they inhibit two key effector caspases, caspase-3 and caspase-7, and the key initiator caspase, caspase-9, which is responsible for the intrinsic mitochondrial death pathway triggered by chemotherapy and radiotherapy. In addition, IAPs effectively block the extrinsic, death receptor–mediated cell death pathway [triggered by Fas ligands, tumor necrosis factor–related apoptosis-inducing ligand (TRAIL), and other ligands] by inhibiting caspase-3 activity, the target of activated caspase-8 (6).

XIAP is recognized to be the most potent member of the IAP family with respect to caspase inhibition, with K_is in the high picomolar range, and its overexpression provides the greatest protection for cells both *in vitro* and *in vivo* from apoptotic events and conditions. There is growing evidence that activity of XIAP, and perhaps other IAPs, extends beyond the inhibition of caspases and that multiple cellular events may contribute to the overall antiapoptotic activity of XIAP (7).

Authors' Affiliations: [1]Aegera Therapeutics, Inc., Montreal, Quebec, Canada; [2]Idera Pharmaceuticals, Inc., Cambridge, Massachusetts; and [3]Department of Pharmacology and Toxicology, University of Alabama at Birmingham, Birmingham, Alabama

Received 3/21/06; revised 5/17/06; accepted 6/15/06.

The costs of publication of this article were defrayed in part by the payment of page charges. This article must therefore be hereby marked *advertisement* in accordance with 18 U.S.C. Section 1734 solely to indicate this fact.

Requests for reprints: Jon P. Durkin, Aegera Therapeutics, Inc., 810 Chemin du Golf, Ile des Soeurs, Montreal, Quebec, Canada H3E 1A8. Phone: 514-288-5532; Fax: 514-288-9280; E-mail: jon.durkin@aegera.com.

doi:10.1158/1078-0432.CCR-06-0608

A wide range of evidence suggests that cancer cells use XIAP, and perhaps other IAPs, to evade extrinsic (death receptor–mediated) and intrinsic (mitochondria-mediated) apoptotic cues that normally would cause their demise. XIAP mRNA or protein is overexpressed relative to levels found in normal tissues in all 60 cell lines of the National Cancer Institute tumor cell line panel (8, 9). Overexpression of XIAP has been observed in prostate, pancreatic, gastric, and colorectal cancers, glioblastoma, and acute myelogenous leukemia (AML); (refs. 5, 10). XIAP levels are also elevated in malignant cells isolated from effusions around ovarian, lung, and breast tumors (11). In AML, XIAP overexpression has been associated with poor clinical outcome (9, 12). XIAP expression is also reported to be elevated in AML blasts and biphenotypic blasts from acute mixed lineage leukemia that are associated with the chemotherapy-resistant nature of these diseases (13). Furthermore, XIAP expression increases from the preleukemic disease, myelodysplastic syndrome, to the overt form of AML, a finding consistent with a role for XIAP in transformation and/or therapy resistance (14). A gene profile analysis of >16,000 genes from 218 tumor samples identified XIAP as one of the major genes in a cluster that accurately predicted ovarian carcinomas (15). Furthermore, XIAP expression has been identified as an independent, unfavorable, prognostic indicator for clear cell renal carcinoma (16, 17). These data suggest that inhibition of cellular XIAP activity, specifically in cancer cells under stress and primed for apoptosis due to genetic and chromosomal aberrations, would facilitate the execution of the proapoptotic signals capable of tipping the balance toward death, when challenged by chemotherapeutic agents.

AEG35156/GEM 640 (hereafter called AEG35156) is an anti-XIAP antisense oligonucleotide synthesized with second-generation antisense chemistry. It is a 19-mer, fully phosphorothioated (replacement of a nonbridging oxygen in the normal phosphate backbone with sulfur) oligonucleotide in which the core 11 DNA bases are flanked by four 2′-*O*-methyl-modified RNA residues at the 3′ and 5′ ends. The sequence of this mixed backbone oligonucleotide (MBO) was optimized for specificity and cellular potency in the absence of CpG residues to eliminate activities that may arise from CpG-mediated immunostimulation (18). Extensive nonclinical and clinical publications attest to the safety and efficacy of antisense compounds with second-generation chemistry (19, 20).

In this report, we describe a broad set of *in vitro* and *in vivo* preclinical studies that show that inhibition of XIAP expression by AEG35156 enhances apoptosis in cancer cells and results in antitumor activity either as a single agent or in conjunction with clinically relevant chemotherapeutic regimens. AEG35156 is currently being evaluated in phase I clinical trials in humans as either a single agent or in combination with docetaxel or idarubicin/cytarabine (for AML) based in part on the preclinical results presented here.

Materials and Methods

Antisense and control oligonucleotides. Oligonucleotides used in the study include AEG35156 (XIAP antisense), AEG35157 (reversed control), AEG35187 (scrambled control), AEG35191 (4-base mismatch), and AEG35185/Hyb931a (nonsense control). All the oligonucleotides used in this study are 19-mer fully phosphorothioated MBOs with four 2′-*O*-methyl RNA bases at both 5′ and 3′ ends. Oligonucleotides were synthesized using β-cyanoethylphosphoramidite chemistry on a PerSeptive Biosystems 8909 Expedite DNA synthesizer (Boston, MA) as described earlier (19). After the synthesis, oligonucleotides were deprotected using standard protocols, purified by high-performance liquid chromatography, and dialyzed against USP quality sterile water for irrigation (Braun, Bethlehem, PA). The oligonucleotides were lyophilized and dissolved again in distilled water and the concentrations were determined by measuring the UV absorbance at 260 nm. All the oligonucleotides synthesized were characterized by capillary gel electrophoresis and matrix-assisted laser desorption ionization time-of-flight mass spectrometry (Voyager DE STR Biospectrometry Workstation, Applied Biosystems, Foster City, CA) for purity and molecular mass, respectively. The purity of full-length oligonucleotides ranged from 90% to 95% accompanied by small quantities of synthetic product reduced by one or two nucleotides ($n - 1$ and $n - 2$) as determined by capillary gel electrophoresis and/or denaturing PAGE. Some batches of the oligonucleotides were obtained from Integrated DNA Technologies (Coralville, IA) or Biosource (Camarillo, CA).

Cancer cell lines. For *in vitro* studies, cell culture medium and fetal bovine serum (FBS) were purchased from Invitrogen (Burlington, Ontario, Canada). The human pancreatic carcinoma cell line Panc-1 and the human prostate carcinoma cell line PC-3 were obtained from American Type Culture Collection (Manassas, VA) and maintained in DMEM and Ham's F-12 supplemented with 10% FBS, respectively. The cisplatin-resistant human ovarian carcinoma cell line A2780-cp was generously supplied by Dr. T. Chow (Montreal General Hospital, McGill University) and maintained in RPMI 1640 supplemented with 10% FBS. The human non–small cell lung carcinoma cell line NCI-H460 was kindly provided by Dr. Gerald Batist (Lady Davis Institute/Jewish General Hospital, McGill University) and maintained in RPMI 1640 supplemented with 10% FBS. The human breast cancer cell line MDA-MB-231 was supplied by Dr. C. Pratt (University of Ottawa) and maintained in low-glucose DMEM supplemented with 5% FBS. All cell lines were incubated at 37°C in a humidified atmosphere containing 5% CO_2. Cell lines (LS174T and PC-3) for xenograft studies were purchased from American Type Culture Collection and cultured following the manufacturer's instructions (20–23). H460 cells (American Type Culture Collection) were plated in 850 cm^2 roller bottles using RPMI 1640 containing 10% FBS, 1% penicillin/streptomycin, and 1% L-glutamine. Cells were trypsinized, counted, and resuspended in serum-free medium at a concentration of 10 million cells/1 mL for xenograft studies.

Xenograft models. Athymic nude (*nu/nu*) mice (4-6 weeks old) for the cancer xenograft models were purchased from Frederick Cancer Research and Development Center (Frederick, MD). The animal use and care protocol was approved by the Institutional Committee for Animal Use and Care of the University of Alabama at Birmingham and all procedures were done according to the relevant guidelines of NIH/Department of Human and Health Services. For the PC-3 human prostate cancer establishment model (22, 23), male athymic nude (*nu/nu*) mice were injected s.c. with 5×10^6 cells in FBS-free Ham's F-12K and Matrigel (Matrigel basement membrane matrix, Becton Dickinson Labware, Bedford, MA) into the left inguinal area. Animals were randomly divided into treatment and control groups (8-12 animals per group) and treatment was initiated on day 1 (24 hours after cell injection). Sterile 0.9% NaCl solution for the control group and the test MBOs (aseptically dissolved in 0.9% NaCl solution) for the treatment groups were given by i.p. injection at five doses weekly for 6 weeks. For the PC-3 human prostate cancer regression model, the animals were injected with PC-3 cells as described above, but tumors were allowed to establish for 5 days (mean tumor size, ~70 mm^3) before treatment commenced on day 0. Random groups of six animals each were injected with sterile 0.9% NaCl solution for the control group and MBOs for the treatment groups as described in the establishment model. For the combination models, carboplatin (Bristol-Myers Squibb Co., Princeton, NJ) at 120 mg/kg in 0.9% NaCl solution was given i.p. on day 4 or Taxotere (Aventis,

Bridgewater, NJ) at 15 mg/kg (dissolved in polysorbate 80, ethanol, and water) on days 4 and 11.

For the LS174T human colon cancer xenograft establishment model (20), female athymic nude mice were injected s.c. with 3×10^6 cells resuspended in FBS-free MEME and Matrigel into the left inguinal area. Treatment with 0.9% NaCl solution or MBOs i.p. at various doses was initiated on day 2 and continued for 3 weeks at five doses weekly. The animals in all models were monitored by general clinical observation, body weight, and tumor growth. Tumor growth for all xenograft studies was monitored by caliper measurements of two perpendicular diameters, and tumor size (mm^3) was calculated using the formula: $1/2a \times b^2$, where where a is the long diameter and b is the short diameter (mm).

For the H460 lung carcinoma xenograft regression model, female, CD-1 *nu/nu* mice (Charles River, Saint-Constant, Quebec, Canada) were anesthetized with isofluorane, and 1×10^6 cells were injected subdermally on the right flank. Animals were assessed for tumor growth and general health 3 days weekly, with tumor size calculated as $(A \times B)^2 / 2$, where A is the longest dimension and B is the width. On day 11, when tumors were ~40 mm^3, drug treatments began. Docetaxel (30 mg/kg i.p.) or cisplatin (6 mg/kg i.p.) was given as two injections 1 week apart. AEG35156 and AEG35187 treatments were also started on day 11 and continued for 5 days on, 2 days off for the balance of the experiment.

MBO transfection and XIAP mRNA quantification by real-time quantitative reverse transcription-PCR. Depending on the cell line, 1.5×10^4 to 3×10^4 cells per well were seeded into 96-well plates and incubated overnight and transfected with 8 to 500 nmol/L control or antisense MBO and 0.8 μL/well LipofectAMINE 2000 (Invitrogen) according to the manufacturer's protocol. After 8 hours of transfection, H460 and A2780-cp cells were harvested for total RNA extraction. For Panc-1, MDA-MB-231, and PC-3 cells, the transfection mixes were replaced with normal medium after 8 hours and harvested 12 hours later. Total RNA was extracted using the RNeasy 96 kit (Qiagen, Mississauga, Ontario, Canada) according to the manufacturer's protocol for use with the QIAvac 96 vacuum manifold. XIAP mRNA levels were determined using real-time quantitative reverse transcription-PCR (RT-PCR). The forward (5′-GGTGATAAAGTAAAGTGCTTTCACTGT-3′) and reverse (5′-TCAGTAGTTCTTACCAGACACTCCTCAA-3′; both from Qiagen) primers were designed to hybridize to exon 3 and a region spanning exons 4 and 5, respectively. The human XIAP probe (5′-FAM-CAACATGCTAAATGGTATCCAGGGTGCAAATATC-3BHQ-1-3′; Integrated DNA Technologies) hybridizes to a region spanning exons 3 and 4. Briefly, the RNA was reverse transcribed and amplified in an ABI PRISM 7700 Sequence Detection System using the Taqman EZ RT-PCR Core Reagent kit and the human glyceraldehyde-3-phosphate dehydrogenase (GAPDH) control reagents (Applied Biosystems) for normalization of XIAP levels to GAPDH mRNA content (24). XIAP levels were expressed as fold increases versus endogenous levels. Real-time RT-PCR analysis of HIAP2 expression was done under identical conditions as those for XIAP, with the exception of using HIAP2-specific primers and probes. The forward (5′-TCTGGAGATGATCCATGGG-TAGA-3′) and reverse (5′-TGGCCTTTCATTCGTATCAAGA-3′) primers were both synthesized by Qiagen, whereas the probe (5′-FAM-CTCACACCTTGGAAACCACTTGGCATG-TAMRA-3′), which spans the exon 3/4 boundary, was synthesized by Applied Biosystems.

XIAP protein quantification by Western blot analysis. For a XIAP protein knockdown time course, H460 cells were seeded at 4.2×10^5 per well into six-well plates and incubated overnight. They were transfected with 31 nmol/L control or antisense MBO and 13.6 μL/well LipofectAMINE 2000 for 18 hours each, on 3 consecutive days, according to the manufacturer's protocol. Sets of samples were harvested after 24, 48, and 72 hours after the first, second, and third transfections, respectively. For a time course on XIAP protein knockdown and poly(ADP-ribose) polymerase (PARP) expression during TRAIL exposure, Panc-1 cells were seeded at 4×10^5 per well into six-well plates and grown overnight. They were transfected with 100 nmol/L control or antisense MBOs and 10 μL/well LipofectAMINE 2000 for 5 hours on 2 consecutive days. After the second transfection, the cells were exposed to 100 ng/mL TRAIL (recombinant human TRAIL/TNFSF10, R&D Systems, Minneapolis, MN) and samples were harvested after 3, 7, and 20 hours. Cell pellets were homogenized in radioimmunoprecipitation assay buffer and the concentration of total protein in the lysates was determined using the Bio-Rad Protein Assay (Bio-Rad, Hercules, CA) according to the manufacturer's protocol. Protein samples were separated on 10% SDS polyacrylamide gels using a Bio-Rad Mini-PROTEAN setup and transferred to Immobilon-P membrane (Millipore, Billerica, MA) in a SemiPhor semidry transfer unit (Hoefer, San Francisco, CA) using standard protocols. Membranes were blocked in a 5% skim milk/TBS-Tween 20 buffer and subsequently incubated with monoclonal mouse anti-hILP/XIAP clone 28 (BD Biosciences, Bedford, MA) or monoclonal mouse anti-GAPDH clone 6C5 (Advanced ImmunoChemical, Inc., Long Beach, CA) and anti-mouse IgG horseradish peroxidase–conjugated secondary antibody (Amersham Biosciences, Piscataway, NJ; ref. 24). For PARP detection, membranes were incubated with rabbit anti-PARP antibody (Cell Signaling Technology, Beverly, MA) followed by donkey anti-rabbit Ig horseradish peroxidase–linked whole antibody (Amersham Biosciences). Signal detection and enhancement was carried out with enhanced chemiluminescence Western blotting detection reagents and exposure on Hyperfilm enhanced chemiluminescence (all reagents were from Amersham Biosciences). Films were scanned using a Hewlett-Packard Scan Jet 4C/T flatbed scanner (Palo Alto, CA) and analyzed with NIH Scion Image Version Beta 4.02 software.

Cell viability assays. H460 or Panc-1 cells were seeded at 1.2×10^4 or 2.5×10^4 per well into 96-well plates, respectively, and grown overnight. They were transfected with either 30 or 100 nmol/L control or antisense MBO, respectively, and 0.5 or 0.8 μL/well LipofectAMINE 2000, respectively, for 5 hours each on 2 consecutive days. On the second day, after the second and last transfections, the cells were exposed to either medium alone for the controls or medium containing 1, 10, or 100 ng/mL TRAIL. A WST-1 cell viability assay (Roche, Mannheim, Germany) was carried out 18 to 20 hours later. The absorbance was measured in an E_{max} plate reader (Molecular Devices, Sunnyvale, CA) at 450 nm with a reference wavelength of 650 nm, and the data were analyzed using Softmax PRO 2.2.1 software.

Mouse splenomegaly assay. Female BALB/c mice (4-6 weeks, 19-21 g; Taconic Farms, Germantown, NY) were injected s.c. with 5 mg/kg AEG35156 or an immunostimulatory 18-mer phosphorothioate oligonucleotide (25) or 0.9% NaCl solution (PBS). The oligonucleotides were dissolved in sterile PBS. After 72 hours, the mice were sacrificed and the spleens were harvested, blotted dry, and weighed.

Immunohistochemistry. Nude mice bearing H460 tumors were treated with 25 mg/kg AEG35156 or 0.9% NaCl solution vehicle i.p. for 8 consecutive days. Tumors were excised, fixed, paraffin embedded, and then sectioned and stained with a monoclonal antibody specific for XIAP (BD Biosciences, Bedford, MA) (clone 48, 1:50 dilution). Sections were dewaxed and processed by antigen retrieval in a microwave. Following blocking for endogenous mouse IgG and peroxidase, sections were stained with clone 48 followed by anti-mouse horseradish peroxidase. Enzyme catalyzed deposition of tyramide-biotin was followed by treatment with horseradish peroxidase-streptavidin and 3,3′-diaminobenzidine staining. Hematoxylin counterstaining was applied.

RNase H assay. HeLa cervical carcinoma cell total RNA (20 μg) was preincubated with 0.2 μmol/L AEG35156 for 5 minutes at 65°C (to denature RNA) and then chilled on ice for 2 minutes. Recombinant RNase H (5 units; New England Biolabs, Pickering, Ontario, Canada) was added after a 2-minute incubation at 37°C; a time course of 0, 20, 60, and 120 minutes at 37°C was initiated for the enzymatic reaction. At the end of the incubation, RNase H was inactivated by heating at 65°C for 20 minutes. RNA was run through a RNA cleanup procedure using Qiagen RNeasy MinElute column (Qiagen) before mRNA analysis. Real-time quantitative RT-PCR analyses (Taqman) were done in triplicate for XIAP, HIAP2/cIAP1, and GAPDH in two separate multiplexed reactions as described above.

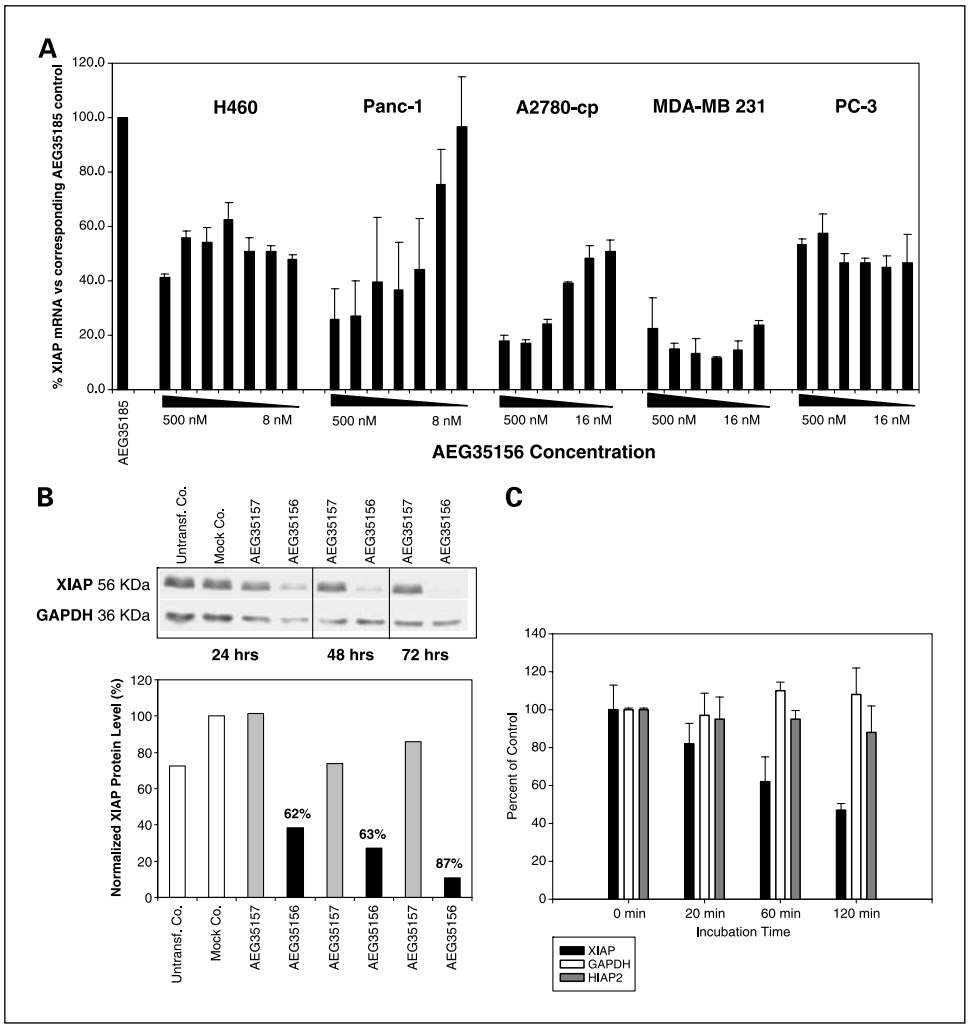

Fig. 1. AEG35156 antisense shows potent mRNA and protein knockdown of XIAP *in vitro*. *A,* different cell lines (H460, Panc-1, A2780cp, MDA-MB-231, and PC-3) were transfected as described in Materials and Methods with increasing doses of AEG35156 (8 or 16, 31, 62, 125, 250, and 500 nmol/L) and XIAP mRNA levels were measured by quantitative RT-PCR after 8 to 24 hours. Columns, percent XIAP mRNA levels for each dose of antisense relative to the corresponding dose of control oligonucleotide (AEG35185) for each cell line; bars, SD. *B,* H460 cells were transfected daily for 1, 2, or 3 days with 31 nmol/L AEG35156 or the control oligonucleotide, AEG35157, and XIAP protein was detected by Western blot at 24, 48, and 72 hours. Percent knockdown of XIAP protein was determined densitometrically, normalized to GAPDH, and expressed relative to values obtained using the control oligonucleotide. *C,* purified total cellular RNA was incubated *in vitro* at 37°C for 0 to 120 minutes with 200 nmol/L AEG35156 and purified recombinant RNase H, after which the reaction was stopped and XIAP levels were measured. XIAP (*black columns*), HIAP2/cIAP1 (*gray columns*), and GAPDH (*white columns*) mRNA levels were measured in multiplex reactions by quantitative RT-PCR. Columns, mean relative to values obtained at $t = 0$; bars, SD.

Results

AEG35156 antisense suppresses XIAP mRNA and protein *in vitro*

AEG35156 was selected from cellular-based screens comparing >100 different antisense oligonucleotide sequences[4] and nominated as a clinical development candidate based on the promising *in vitro* and *in vivo* results shown below.

AEG35156 effectively down-regulated XIAP mRNA expression in *in vitro* transfection studies with multiple human cancer cell lines derived from cancers of the lung (H460), pancreas (Panc-1), ovary (A2780-cp), breast (MDA-MB-231), and prostate (PC-3; Fig. 1A). XIAP mRNA levels at each concentration of AEG35156 were normalized to XIAP RNA levels observed using the same concentration of a nonsense control oligonucleotide sequence (AEG35185). AEG35156 caused the down-regulation of XIAP mRNA with an EC_{50} in the range of 8 to 32 nmol/L for H460, Panc-1, A2780cp, and PC-3 cells, and the EC_{50} in MDA-MB-231 was significantly below the lowest tested concentration of 16 nmol/L. Panc-1 and A2780cp cells showed a dose-dependent reduction in XIAP-mRNA, whereas the other cell lines caused a suppression of XIAP mRNA in the low nanomolar range without a clear dose response at higher doses. By comparison, the nonsense control oligonucleotide, AEG35185, in the EC_{50} range for AEG35156 (i.e., 8-32 nmol/L) reduced XIAP mRNA levels by 8.7 ± 14% for the five cell lines tested (data not shown).

AEG35156 produced a dose- and time-dependent reduction of XIAP protein in H460 cells after one or repeated transfections over a 24- to 72-hour period (Fig. 1B). Repeated transfections caused a progressive loss of XIAP protein with a near-complete loss achieved (87%) by 72 hours relative to a reverse polarity control oligonucleotide AEG35157. Other cells lines, including Panc-1, PC-3, and A2780cp, also showed substantial losses of XIAP protein (50-72%) when treated with 16 to 31 nmol/L AEG35156 as a double transfection (data not shown).

The chimeric nature of MBOs is purposely designed to enhance stability to nucleases while maintaining RNase H–activating properties of the antisense mRNA target duplex (19). RNase H activation is the principal mechanism by which antisense oligonucleotides degrade target mRNAs once the antisense hybridizes to the target region. Mixing AEG36156 with recombinant RNase H in a total cellular RNA extract caused a selective and progressive loss of XIAP mRNA (Fig. 1C). The selectivity of this RNase H activity was shown by the fact that

[4] Unpublished results.

neither GAPDH-mRNA or the mRNA of another IAP family member, cIAP1, underwent similar degradation under the conditions employed (Fig. 1C). These data are consistent with the loss of XIAP-mRNA and protein observed in cells by AEG35156 being mediated principally via a RNase H mechanism.

AEG35156 enhances sensitization of Panc-1 pancreatic carcinoma cells to TRAIL-induced cell death

Growing evidence indicates that XIAP activity is effective in blunting extrinsic death stimuli, particularly TRAIL-induced apoptosis (6, 26–33). The effect of suppressing XIAP levels on the sensitivity to the death receptor agonist TRAIL was assessed in Panc-1 cells. As shown in Fig. 2A, Panc-1 cells are highly resistant to TRAIL at concentrations up to 100 ng/mL. Similarly, AEG35156 had no effect on Panc-1 cell survival when used at 100 nmol/L (data not shown). However, when applied in combination, AEG35156 (100 nmol/L) sensitized cells to TRAIL, causing a dose-dependent cell death that reached 63% of the population at 100 ng/mL TRAIL. This sensitization to TRAIL was not observed in Panc-1 cells treated with the control MBO, AEG35157, relative to untransfected cells or cells subjected to a mock transfection (Fig. 2A). The TRAIL-sensitizing effect of AEG35156 was also observed in H460 cells (Fig. 2B), which are intrinsically more sensitive to TRAIL than Panc-1 cells. AEG35156, at 30 nmol/L, sensitized cells to TRAIL, causing a dose-dependent cell death that reached 62% of the population at 10 ng/mL TRAIL (Fig. 2B).

The synergistic effects of TRAIL and AEG35156 on Panc-1 cell death correlated with the progressive loss of XIAP protein and increased PARP cleavage (Fig. 2C). TRAIL alone (100 ng/mL; lanes 2 and 3) had little effect on the levels of XIAP protein, only marginal effects on PARP cleavage over the 20-hour time course, and caused the death of ~15% of the cell population. However, TRAIL added to cells in which a moderate reduction (~40% by densitometric analysis) of XIAP protein was induced by AEG35156 (lane 5; 0 time) caused a significant time-dependent cleavage of PARP (lane 5) most likely due to the effects of active caspase-3 and/or caspase-7 released from XIAP inhibition. TRAIL also caused a further time-dependent decrease in XIAP protein levels (lane 5; i.e., up to 90% by densitometric analysis at 20 hours) possibly through a feed-forward amplification loop initiated by caspase activities.

AEG35156 shows antitumor effects *in vivo* as a single agent and in combination with docetaxel

AEG35156 was tested in three different xenograft models of human prostate, colon, and lung cancers (i.e., PC-3, LS174T, and H460, respectively) either as a single agent or in combination with clinically relevant chemotherapeutics.

LS174T human colon cancer xenografts. LS174T xenografts were established by s.c. injection of cells into the left inguinal

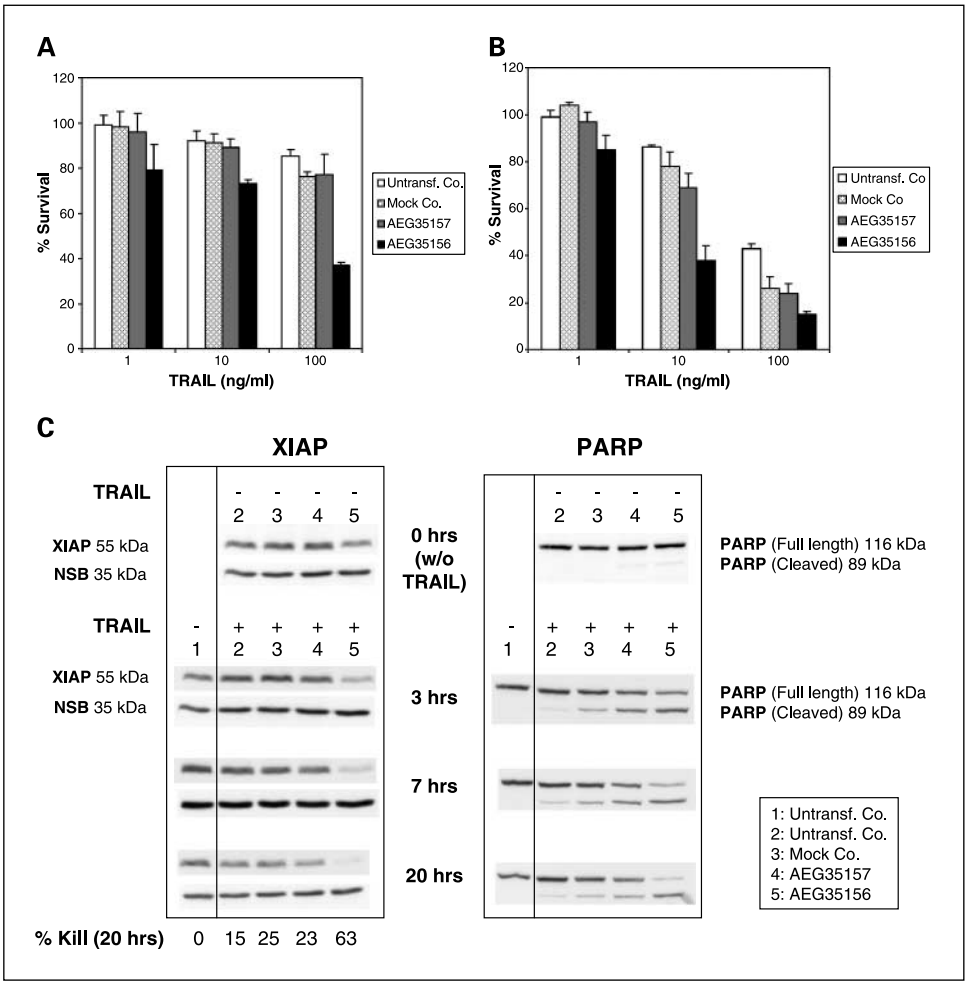

Fig. 2. AEG35156 enhances apoptosis and sensitizes PANC-1 and H460 cells to TRAIL *in vitro*. *A,* survival of Panc-1 human pancreatic cancer cells following double transfection over a 2-day period with 100 nmol/L AEG35156, 100 nmol/L control oligonucleotide (AEG35157), or LipofectAMINE 2000 alone (mock) followed by a 20-hour exposure to the indicated doses of TRAIL. Columns, percent survival of cells compared with non-TRAIL-treated cells; bars, SD. *B,* survival of H460 human non – small cell lung cancer cells following double transfection over a 2-day period with 30 nmol/L AEG35156, 30 nmol/L control oligonucleotide (AEG35157), or LipofectAMINE 2000 alone followed by a 20-hour exposure to the indicated doses of TRAIL. Columns, percent survival of cells compared with non-TRAIL-treated cells; SD. *C,* time-course study of untreated Panc-1 cells (*lanes 1* and *2*) and Panc-1 cells transfected over a 2-day period with 100 nmol/L AEG35156, 100 nmol/L control oligonucleotide (AEG35157), or LipofectAMINE 2000 alone followed by exposure to vehicle (*lane 1*) or 100 ng/mL TRAIL (*lanes 2-5*) for 3 to 20 hours. Western blots show specific XIAP protein loss with AEG35156, which correlated with the increased appearance of caspase-specific PARP cleavage product (89 kDa) and cell death observed at 20 hours by WST-1 staining (*% Kill*). A nonspecific band (*NSB*) was used as a protein loading control.

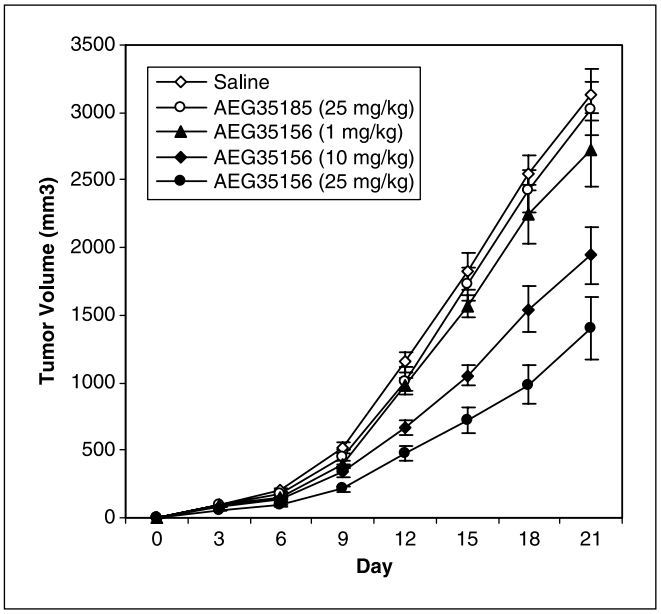

Fig. 3. Dose-dependent single-agent antitumor effects of AEG35156 in a LS174T colon cancer xenograft (establishment) model. Dose-dependent antitumor effect of AEG35156 as a single agent in nude mice implanted with LS174T human colon carcinoma cells. As described in Materials and Methods, animals were treated i.p. with AEG35156 at 1, 10, or 25 mg/kg body weight/d on a 5 days on, 2 days off regimen for 3 weeks. The control oligonucleotide, AEG35185, was given at 25 mg/kg body weight/d. Points, mean (n = 10 per group); bars, SE.

area of female athymic nude mice. Injected animals were randomized into treatment and control groups, and AEG35156 treatment initiated on day 3 by i.p. injection at 1, 10, or 25 mg/kg body weight/d, five doses weekly. Control groups received sterile 0.9% NaCl solution or a nonsense control sequence, AEG35185, by i.p. injection at 25 mg/kg body weight/d, five doses weekly. Tumor measurements are presented in Fig. 3. Tumor growth in AEG35185-treated animals was not different from that in the 0.9% NaCl solution control group. By contrast, AEG35156 exhibited a dose-dependent inhibitory effect on tumor growth, with a 60% reduction in tumor volume relative to the 0.9% NaCl solution control group observed at the highest dose given. Tumor growth inhibition was observed within 3 days of initiating AEG35156 treatment on day 3.

H460 human lung cancer xenografts. H460 xenografts were established by s.c. injection of cells into the right flank of female athymic nude mice. On day 11, tumor-bearing animals were assigned to treatment groups, such that each group had a similar mean tumor size of ~40 mm^3. AEG35156 treatment was initiated by i.p. injection on day 11 at 10 or 25 mg/kg body weight/d, five doses weekly. Control groups received sterile 0.9% NaCl solution alone or a scrambled control sequence, AEG35187 at 25 mg/kg body weight/d, five doses weekly. Animals received AEG35156 alone or in combination with either docetaxel (30 mg/kg i.p.) or cisplatin (6 mg/kg i.p.) twice, 1 week apart.

In this instance, H460 xenografts were largely refractory to AEG35156 given as a single agent (Fig. 4A). By contrast, AEG35156 given in combination with docetaxel had a dramatic, dose-dependent effect on tumor size, with the 10 mg/kg group exhibiting a 56% reduction in tumor size compared with controls and the 25 mg/kg group in combination with docetaxel having a mean tumor size ~80% smaller than controls (Fig. 4B). This inhibitory effect on tumor growth was a clear example of synergy, because neither the antisense nor the docetaxel dose used (30 mg/kg) was effective as a single agent. The control sequence, AEG35187 in combination with docetaxel, was not different than either saline or docetaxel alone groups. By comparison, the combination of cisplatin with AEG35156 did not show increased antitumor activity (Fig. 4C).

XIAP protein knockdown was observed by immunohistochemistry in tumors excised from H460 xenografts following 8 days of treatment with 25 mg/kg AEG35156 (Fig. 4D). Excised tumors from AEG35156-treated animals showed a substantial reduction in XIAP-specific staining intensity relative to tumors isolated from 0.9% NaCl-treated animals. Background staining is shown in the "no primary" control sections for the respective treatment groups (Fig. 4D).

PC-3 human prostate carcinoma xenografts. PC-3 human prostate cancer xenografts were established in male athymic nude using methods reported previously (22). On the first AEG35156 treatment day (day 0; 5 days after implantation), animals were divided into treatment and control groups so that each group had a similar mean tumor size distribution of 70 mm^3. AEG35156 was given by i.p. injection at 10 or 25 mg/kg body weight/d, 5 days weekly for 6 weeks. AEG35191, a 4-base mismatch to AEG35156, served as a negative control and was given at 25 mg/kg body weight/d, five doses weekly. Some groups received docetaxel (15 mg/kg i.p.) on days 4 and 11 or carboplatin (120 mg/kg i.p.) on day 4.

PC-3 tumor growth in animals treated with the control oligonucleotide, AEG35191, was comparable with that observed with the 0.9% NaCl solution control group (Fig. 5A). By contrast, AEG35156 showed a dose-dependent reduction in the rate of tumor growth, with a ~80% reduction in tumor size reported at the highest dose level. Modest tumor regression was observed over the first 14 days of AEG35156 treatment, where tumor size values were lower than those determined on day 0 (Fig. 5B).

Docetaxel was used at a dose that elicited a ~50% reduction in tumor growth when given as a single agent (Fig. 5C). The combination of AEG35156 and docetaxel showed significantly enhanced and dose-dependent antitumor activity, with complete regression of tumors observed at the 25 mg/kg body weight/d dose level (Fig. 5D). In the study, AEG35156 treatment was curtailed on day 42, and subsequent tumor regrowth was evaluated in the high-dose group for an additional 56 days after stopping antisense treatment (day 98), at which time tumors were only barely perceptible.

Carboplatin was used at a dose and regimen that gave a suboptimal antitumor effect (~30% tumor reduction) when applied as a single agent. As shown in Fig. 5D, the combination of AEG35156 and carboplatin was significantly better than carboplatin alone (~80%) but not substantially better that AEG35156 as a single agent at the same dose (Fig. 5A). Thus, little or no additivity was observed between carboplatin and AEG35156.

Body weight measurements from xenograft studies

General health status and body weight measurements were done for all the xenograft studies. In general, AEG35156 was well tolerated both when given alone or combined with the

chemotherapeutic agents used (Fig. 6). Animals did show signs of weight loss (<10%) after prolonged AEG35156 treatment at 25 mg/kg/d in the PC-3 study (Fig. 6A). This weight loss was not specific to AEG35156, as it was also seen for the control MBO, AEG35191, which showed greater weight loss (Fig. 6A) without significant antitumor activity (Fig. 5A). Animal body weights were observed to recover quickly after antisense treatments were stopped (Fig. 6A and B).

AEG35156 does not show immunostimulatory activity in a splenomegaly assay compared with TLR9-activating immunomers

Although AEG35156 was designed not to contain CpG immune stimulating motifs, an *in vivo* study was undertaken to examine the immunostimulatory activity of AEG35156. AEG35156 (5 mg/kg) or an 18-mer CpG oligonucleotide (25) was injected s.c. into mice and spleen weights were determined 3 days later. AEG35156 produced an insignificant increase (6%) in spleen weight relative to 0.9% NaCl solution injected mice, whereas the CpG oligonucleotide produced an 82% increase in spleen weight (Table 1). These results suggest that AEG35156 exhibits little or no immunostimulatory activity.

Discussion

It is widely recognized that although many cancer cells are primed for apoptosis, they fail to die because of the development of multiple mechanisms preventing final enactment of the death process (34, 35). This is particularly true of tumor cells challenged by chemotherapeutic agents that impart powerful apoptotic signals to proliferating cells. Deregulation of apoptotic pathways seems to be critical for the sustained viability and proliferation of cancer cells and is an important determinant in chemoresistance (4, 34, 35).

The up-regulation of IAPs is viewed as a fundamental means by which many cancer cells evade death even in the presence of strong extrinsic (death receptor–mediated) and intrinsic (mitochondria-mediated) apoptotic cues (1, 6). It is thus reasonable to assert that the inhibition of cellular IAP activity, particularly in cells primed to undergo apoptosis either intrinsically or under chemotherapeutic challenge, should constitute a powerful proapoptotic signal capable of tipping the balance toward death.

Previous proof-of-principle studies have shown the anticancer effects of XIAP antisense or small interfering RNA oligonucleotides in cellular studies representing solid tumors (36–48) and leukemias (49, 50). We have reported previously that a first-generation antisense against XIAP used in combination with vinorelbine caused reductions in tumor growth rate of lung cancer xenografts (51). In addition, experimental small-molecule inhibitors of XIAP have also shown anticancer effects *in vitro* by inducing apoptosis in solid tumor cell lines and leukemia cells (2). In numerous experimental systems, cancer cells induced to apoptose by various agents, a loss of XIAP protein was found to precede cell death, suggesting that removal of XIAP is a prerequisite for the final enactment of cell death.

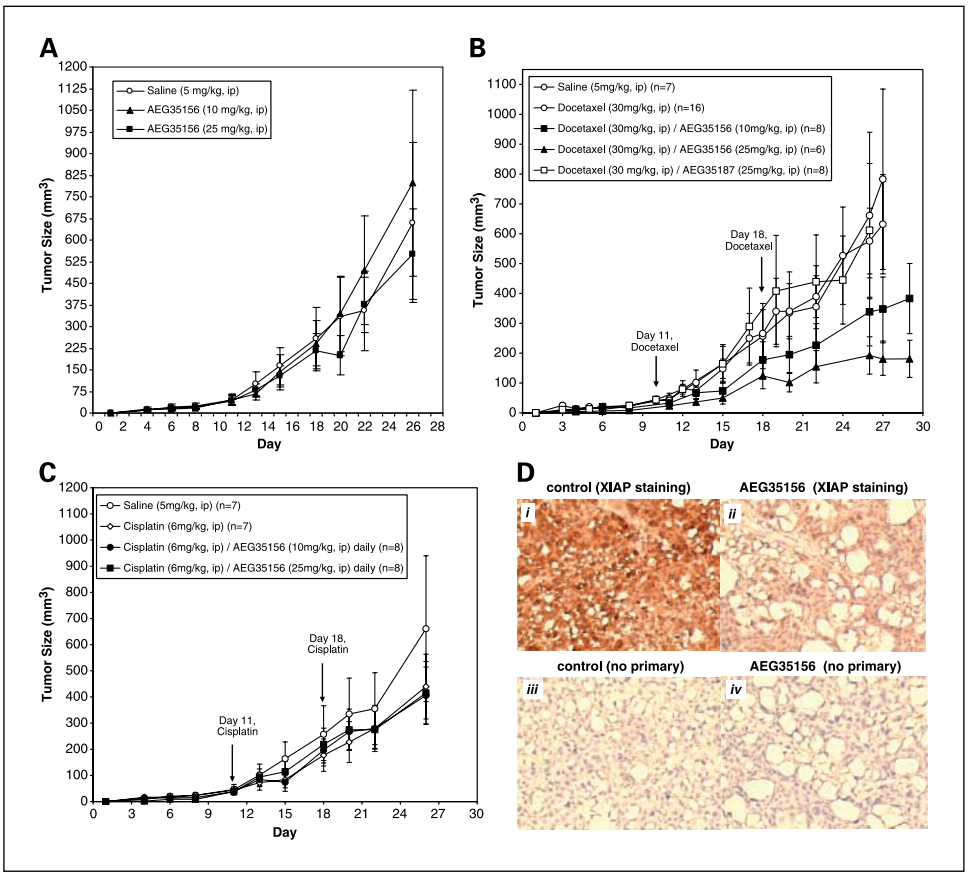

Fig. 4. AEG35156 effects on H460 tumor growth in combination with docetaxel or cisplatin. Dose-dependent antitumor effect of AEG35156 as single agent (*A*) or in combination with docetaxel (*B*) or cisplatin (*C*) in nude mice implanted with H460 human lung cancer cells. Animals were treated i.p. with saline vehicle (same curve shown in A, B and C) or AEG35156 at 10 or 25 mg/kg body weight/d with a 5 days on, 2 days off regimen for 3 weeks. Tumors were allowed to grow for 11 days until they reached a palpable size (~40 mm^3) before initiating antisense treatment. Day 1 is the day of cell implantation. The antisense treatment period was from days 11 to 27. Docetaxel (30 mg/kg i.p.) was given on days 11 and 18 and cisplatin (6 mg/kg i.p.) was given on days 11 and 18. The control oligonucleotide, AEG35187, was given by the same regimen at 25 mg/kg/d in combination with docetaxel. Points, mean (n = 6-8 animals per group); bars, SE. *D,* H460 tumor-bearing athymic nude mice were treated for 7 consecutive days with saline or AEG35156 (25 mg/kg i.p.). Twenty-four hours after the seventh injection, animals were euthanized and the tumors were excised, fixed, and sectioned. Immunohistochemical staining for XIAP revealed a marked decrease in XIAP after antisense treatment.

We undertook the development of an optimized second-generation antisense against XIAP to directly test this hypothesis in xenograft models representing major cancer types. AEG35156 was capable of reducing XIAP cellular mRNA levels by ≥50% in transfection reactions at doses between 8 and 32 nmol/L (Fig. 1A). This represents a substantial improvement over our best first-generation XIAP antisense that was effective in the high nanomolar to low micromolar range under comparable transfection conditions (51). These improvements in potency are presumably due, in part, to the increased stability of second-generation chemistries and the selection of an optimal sequence. Repeated daily transfections of H460 cells at low dose (31 nmol/L) resulted in a nearly complete (87%) suppression of XIAP protein levels after 72 hours (Fig. 1B). We have found that the repeated transfections of AEG35156 (two to three times before harvesting samples for *in vitro* experiments) allows for a more profound knockdown of the target compared with a single transfection (Fig. 1B). This is likely due to the required continued exposure to the antisense and the time needed for mRNA and protein turnover to occur. The AEG35156-mediated loss of XIAP protein could result in part from translational interference or altered splicing because AEG35156 spans an exon-intron boundary. However, AEG35156 did specifically result in the loss of XIAP mRNA in transfection reactions (Fig. 1A) and was able to induce RNase H–mediated degradation of XIAP message in a pool of total RNA, whereas two nontargeted sequences (HIAP2/cIAP1 and GAPDH) remained intact (Fig. 1C). Hence, RNase H–mediated degradation of the XIAP mRNA complexed to AEG35156 is most likely the principal mechanism for the observed loss of XIAP protein in cells and tumors.

The effectiveness of death receptor agonists, such as TRAIL, Fas, and tumor necrosis factor-α, to evoke apoptosis is substantially influenced by the status of XIAP in cells (e.g., refs. 27, 31, 52–54). We have reported previously that XIAP overexpression protects against TRAIL-induced killing (reviewed in ref. 6) and that XIAP depletion by RNA interference sensitizes cells to TRAIL-induced death (30, 40). In the present study, TRAIL-sensitive H460 cells and TRAIL-resistant Panc-1 cells were sensitized to 10 or 100 ng/mL TRAIL by AEG35156 (Fig. 2A and B), respectively. In addition, Panc-1 cells were sensitized when XIAP protein levels were partially depleted (~40%) with AEG35156 (63% cell death) compared with a control oligonucleotide (23% cell death; Fig. 2C). Although XIAP does not directly inhibit caspase-8, the apical caspase activated by TRAIL, it inhibits caspase-3, the downstream effector of activated caspase-8. XIAP also inhibits caspase-9 under conditions where caspase-8-mediated Bid cleavage results in the release of cytochrome *c* and activation of caspase-9 (i.e., in type II cells). The addition of TRAIL to XIAP-depleted Panc-1 cells resulted in enhanced caspase-3 activity as detected by the appearance of a specific PARP cleavage product (89 kDa; Fig. 2C). Moreover, cell death attributed to the combination of TRAIL and AEG35156

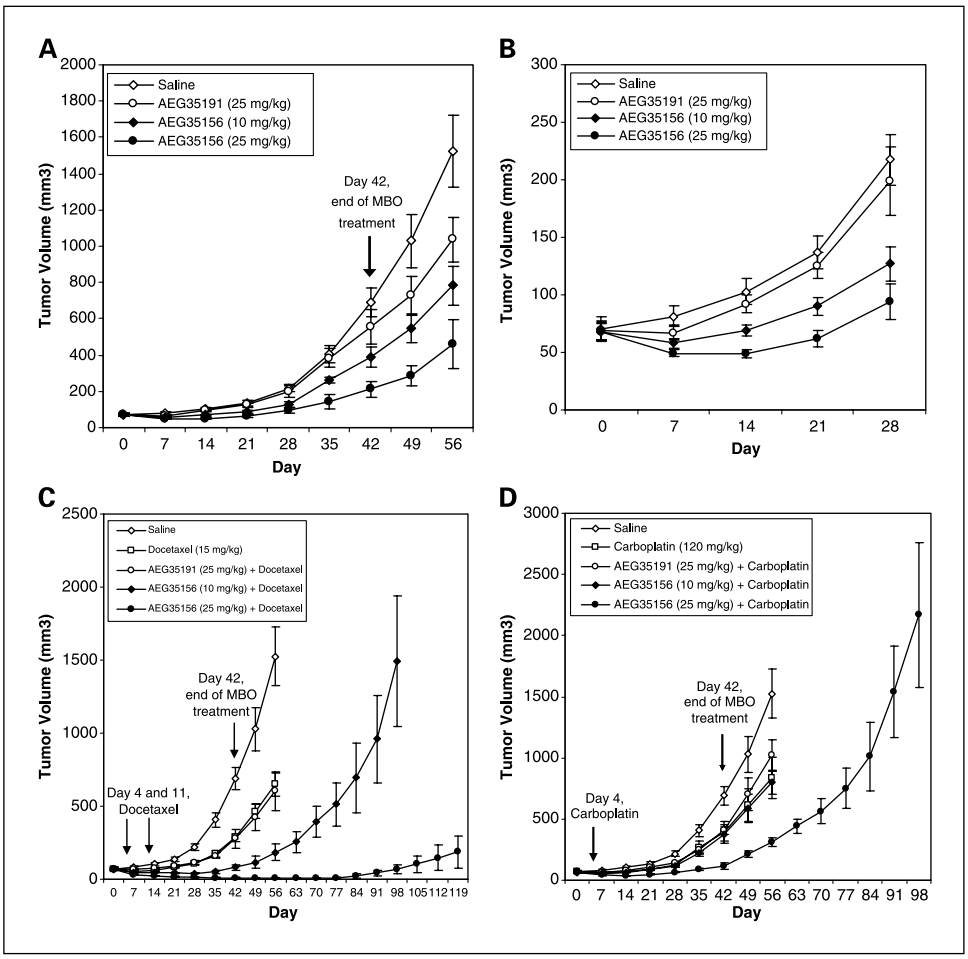

Fig. 5. AEG35156 shows dose-dependent single-agent and combination antitumor effects in PC-3 prostate cancer xenograft (regression) model. Dose-dependent antitumor effects of AEG35156 as a single agent [*A*; enlarged view for the single-agent data for days 0-28 (*B*)] or in combination with docetaxel (*C*) or carboplatin (*D*) in nude mice implanted with PC-3 human prostate carcinoma cells. Animals were treated i.p. with 0.9% NaCl solution vehicle, AEG35156 at 10 or 25 mg/kg body weight/d, or the control sequence AEG35191 at 25 mg/kg/d on a 5 days on, 2 days off regimen for 6 weeks. The antisense treatment period was from days 0 to 42. Tumors were allowed to establish to 70 mm^3 for 5 days before initiating antisense or control treatment. Day 0 is the first day of treatment (5 days after cell implantation). Docetaxel was given i.p. at 15 mg/kg on days 4 and 11 and carboplatin was given i.p. at 120 mg/kg on day 4. Points, mean (n = 6 animals per group); bars, SE.

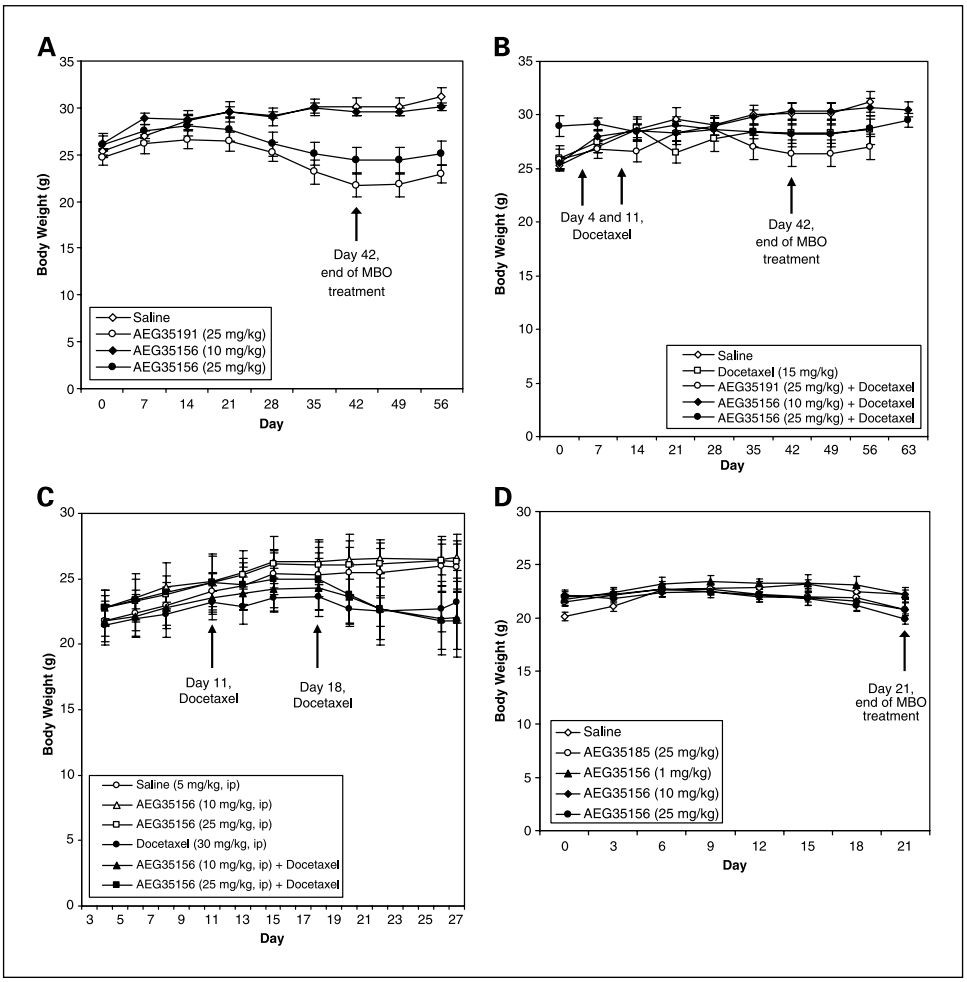

Fig. 6. AEG35156 exhibits minimal *in vivo* toxicity. Animal body weight changes for animals used in the xenograft studies described in Figs. 3 to 5. Corresponding body weight for (*A*) PC-3 xenograft study shown in Fig. 5A, (*B*) PC-3 xenograft study shown in Fig. 5C, (*C*) H460 xenograft study shown in Fig. 4B, and (*D*) LS174T xenograft study shown in Fig. 3.

correlated with further time-dependent losses of XIAP protein. Increased PARP cleavage and XIAP losses were seen as early as 3 hours after TRAIL addition to XIAP-depleted cells (Fig. 2C). It is possible that partial depletion of XIAP by AEG35156 in Panc-1 cells releases sufficient caspase activity in cells to prime death receptor pathways (perhaps via caspase-3-mediated caspase-8 activation) and this process is amplified in a feed-forward manner resulting in further losses of XIAP, enhanced caspase activity, and eventual cell death. In this report, we only show increased sensitization of AEG35156-treated cells to TRAIL for pancreatic carcinoma and non–small cell lung carcinoma cell lines. However, based on previous RNA interference (30) and other XIAP gene ablation approaches (31) in breast cancer (30) and colon cancer (31) cell lines, we believe that XIAP down-regulation by AEG35156 may generally increase TRAIL killing in death receptor–positive cancer cells, although this remains to be proven.

Table 1. Lack of splenomegaly in animals treated with AEG35156 compared with an immunostimulatory oligonucleotide

	MBO dose (mg/kg)	Average spleen weight (mg)	% Weight increase vs PBS
AEG35156	5	92.7 ± 6.6	6.4
(+) Control	5	158.9 ± 14.8	82.4
PBS	—	87.1 ± 5.3	0

In established PC-3 prostate carcinoma xenografts, AEG35156 produced a dose-dependent antitumor effect as a single agent when given as repeat daily dosing (cycles of 5 consecutive treatment days weekly). AEG35156-induced tumor regression was observed during the initial treatment period, resulting in a 2- to 4-week delay in tumor growth (Fig. 5B), whereas the control oligonucleotide had no effect. AEG35156 also showed a dose-dependent single-agent activity against established LS174T colon cancer xenografts (Fig. 3), thus extending the finding of single-agent activity for AEG35156 to a second unrelated cancer cell line. By contrast, in established H460 lung cancer xenografts, AEG35156 failed to show significant single-agent activity. Given the mechanisms by which XIAP and AEG35156 function, it would be expected that the ability of the antisense compound to exact single-agent activity in tumors would be a function of the level of XIAP suppression by AEG35156, and the extent to which cellular caspases are active in the growing tumor mass under AEG35156 treatment conditions.

Although AEG35156 did not exhibit single-agent effects in H460 xenografts, it did show robust, dose-dependent antitumor activity when combined with docetaxel. In this model, where the docetaxel treatment conditions were such that minimal single-agent effects were observed, AEG35156

significantly enhanced the antitumor effects of the taxanes (Fig. 4B). This antitumor activity in H460 xenografts correlated with AEG35156-induced XIAP suppression in tumors excised from mice at an early time point (day 8), measured by immunohistochemistry (Fig. 4D), and immunofluorescence (data not shown). The effectiveness of combining AEG35156 with taxanes was confirmed in the PC-3 xenograft study, where the combination of AEG35156 with docetaxel resulted in long-term sustained tumor regression that persisted well beyond the end of AEG35156 therapy on day 42 (Fig. 5C). The effectiveness of combining XIAP down-regulation with the cytotoxic action of paclitaxel/docetaxel may possibly be explained by the recent finding that in human lymphoblastic leukemia cells, paclitaxel triggers FADD-dependent apoptosis primarily through a direct activation of caspase-10 but independently of death receptors (55). These finding suggest that taxanes, in part, have similarities in action to TRAIL and other death receptor agonists and may explain why AEG35156 and TRAIL (*in vitro*) or docetaxel (*in vivo*) have produced dramatic combinational results in the present study.

Although the results clearly indicate that AEG35156 worked well in concert with taxanes, it was equally apparent that the partnership of AEG35156 with the platinum-based drugs, cisplatin and carboplatin, was unproductive. In H460 xenografts, AEG35156 failed to sensitize the tumor to cisplatin (Fig. 4C), and in PC-3 xenografts, the combination of carboplatin and AEG35156 suppressed tumor growth to a level no greater than AEG35156 as a single agent (Fig. 5A and D).

In the PC-3 xenograft study, both AEG35156 and the control AEG35191 produce a <10% body weight loss at the highest tested dose, which was reversible on cessation of treatment (Fig. 6A and B). This effect was regarded as a class-related effect of oligonucleotides, which was not associated with the antitumor effects observed for AEG35156, because the control oligonucleotide showed even greater weight loss than AEG35156 (Fig. 6A and B) without significant antitumor effects (Fig. 5A and C). Similar findings where found in the H460 lung xenograft study where a <10% reduction in body weight occurred in the docetaxel/AEG35156 groups relative to the docetaxel group alone but only at times well after the antitumor effects of the combination became apparent (Fig. 6C).

The results presented indicate that AEG35156 effectively reduces XIAP levels in cancer cells in both culture and animal models and that reduction of cellular XIAP protein using an antisense approach is an effective means to sensitize tumors to those chemotherapeutic drugs that mechanistically work in concert with XIAP suppression, such as docetaxel. These results, along with the single-agent activities seen in two of the three xenograft models tested, indicate that lowering the apoptotic threshold of cancer cells by suppressing XIAP activity allows apoptosis to proceed. It should be noted that the plasma bioavailability of antisense oligonucleotides given i.p. has been reported to be <30% of that achieved by i.v. dosing (56). Thus, the efficacious dose range of AEG35156 given i.p. in the various xenograft studies described (10-25 mg/kg/d) would convert to ~3 to 7 mg/kg/d when given by the i.v. route, which is within the dose range reported to be well tolerated in myriad human antisense studies (57).

The *in vivo* studies presented herein were designed as endpoint studies aimed at determining *in vivo* efficacy and safety outcomes and not designed to address mechanistic aspects of AEG35156 action in tumors. We plan to carry out such *in vivo* mechanistic experiments in a separate future study. We have carried out an additional *in vivo* study of AEG35156 in an ovarian carcinoma xenograft survival model[5] and determined the percentage of living versus dead tissue based on H&E staining of tumor cross-sections. AEG35156-treated animals show a decrease in tumor surface area for living cells compared with tumors from control treated animals.[5]

AEG35156 has been evaluated in toxicology studies in support of its clinical development.[6] In brief, a cardiovascular/respiratory/neurologic safety pharmacology study done in monkeys by a 24-hour continuous i.v. infusion regimen (to mimic the regimen used in the first-in-man clinical study) showed AEG35156 to be well tolerated and to be negative in a series of genotoxicity tests. Dose escalating studies conducted in rats and monkeys using three cycles of 7-day continuous i.v. infusion every 21 days showed AEG35156, up to 40 mg/kg/d, to be safe and well-tolerated, largely showing expected class-related toxicities for these types of compounds.

AEG35156 entered the clinic in 2004 in a phase I single agent trial conducted in the United Kingdom in patients with advanced tumors. In 2005, based in part on the positive preclinical pharmacology data presented in this study, a phase I trial of AEG35156 in combination with docetaxel was initiated at multiple Canadian centers. More recently, a phase I/II trial has been initiated to assess AEG35156 in AML patients in combination with cytarabine and idarubicin.

[5] Shaw TJ, LaCasse EC, Durkin JP, Vanderhyden BC. Down-regulation of XIAP expression in ovarian cancer cells induces cell death *in vitro* and *in vivo*, in preparation.
[6] Di Tullio KP, LaCasse EC, Winocour P, et al. Preclinical toxicological, pharmacokinetic and pharmacodynamic studies of a second generation antisense to XIAP, AEG35156/GEM 640, in rodents and cynomolgus monkeys: Demonstration of target knockdown *in vivo*, in preparation.

Acknowledgments

We thank Martine St-Jean and Charles Lefebvre for expert technical assistance and Drs. Gerald Batist and Mustapha Kandouz (Lady Davis Institute/Jewish General Hospital) for excellent advice.

References

1. LaCasse EC, Holcik M, Korneluk RG, MacKenzie AE. Apoptosis in health, disease, and therapy: overview and methodology. In: Holcik M, LaCasse E, MacKenzie A, Korneluk R, editors. Apoptosis in health and disease: clinical and therapeutic aspects. Cambridge: Cambridge University Press; 2005. p. 1–48.
2. Schimmer AD, Dalili S, Batey RA, Riedl SJ. Targeting XIAP for the treatment of malignancy. Cell Death Differ 2006;13:179–88.
3. Wright CW, Duckett CS. Reawakening the cellular death program in neoplasia through the therapeutic blockade of IAP function. J Clin Invest 2005;115:2673–8.
4. Kaufmann SH, Vaux DL. Alterations in the apoptotic machinery and their potential role in anticancer drug resistance. Oncogene 2003;22:7414–30.
5. Wrzesien-Kus A, Smolewski P, Sobczak-Pluta A, Wierzbowska A, Robak T. The inhibitor of apoptosis protein family and its antagonists in acute leukemias. Apoptosis 2004;9:705–15.
6. LaCasse EC, Baird S, Korneluk RG, MacKenzie AE. The inhibitors of apoptosis (IAPs) and their emerging role in cancer. Oncogene 1998;17:3247–59.
7. Lewis J, Burstein E, Reffey SB, Bratton SB, Roberts AB, Duckett CS. Uncoupling of the signaling and caspase-inhibitory properties of X-linked inhibitor of apoptosis. J Biol Chem 2004;279:9023–9.

8. Fong WG, Liston P, Rajcan-Separovic E, St Jean M, Craig C, Korneluk RG. Expression and genetic analysis of XIAP-associated factor 1 (XAF1) in cancer cell lines. Genomics 2000;70:113–22.

9. Tamm I, Kornblau SM, Segall H, et al. Expression and prognostic significance of IAP-family genes in human cancers and myeloid leukemias. Clin Cancer Res 2000;6:1796–803.

10. Takeuchi H, Kim J, Fujimoto A, et al. X-linked inhibitor of apoptosis protein expression level in colorectal cancer is regulated by hepatocyte growth factor/C-met pathway via Akt signaling. Clin Cancer Res 2005;11:7621–8.

11. Wu M, Yuan S, Szporn AH, Gan L, Shtilbans V, Burstein DE. Immunocytochemical detection of XIAP in body cavity effusions and washes. Mod Pathol 2005;18:1618–22.

12. Tamm I, Richter S, Oltersdorf D, et al. High expression levels of X-linked inhibitor of apoptosis protein and survivin correlate with poor overall survival in childhood *de novo* acute myeloid leukemia. Clin Cancer Res 2004;10:3737–44.

13. Nakagawa Y, Hasegawa M, Kurata M, et al. Expression of IAP-family proteins in adult acute mixed lineage leukemia (AMLL). Am J Hematol 2005;78:173–80.

14. Yamamoto K, Abe S, Nakagawa Y, et al. Expression of IAP family proteins in myelodysplastic syndromes transforming to overt leukemia. Leuk Res 2004;28:1203–11.

15. Ramaswamy S, Tamayo P, Rifkin R, et al. Multiclass cancer diagnosis using tumor gene expression signatures. Proc Natl Acad Sci U S A 2001;98:15149–54.

16. Ramp U, Krieg T, Caliskan E, et al. XIAP expression is an independent prognostic marker in clear-cell renal carcinomas. Hum Pathol 2004;35:1022–8.

17. Yan Y, Mahotka C, Heikaus S, et al. Disturbed balance of expression between XIAP and Smac/DIABLO during tumor progression in renal cell carcinomas. Br J Cancer 2004;91:1349–57.

18. Agrawal S, Kandimalla ER. Role of Toll-like receptors in antisense and siRNA. Nat Biotechnol 2004;22:1533–7.

19. Agrawal S, Jiang Z, Zhao Q, et al. Mixed-backbone oligonucleotides as second generation antisense oligonucleotides: *in vitro* and *in vivo* studies. Proc Natl Acad Sci U S A 1997;94:2620–5.

20. Wang H, Cai Q, Zeng X, Yu D, Agrawal S, Zhang R. Anti-tumor activity and pharmacokinetics of a mixed-backbone antisense oligonucleotide targeted to RIα subunit of protein kinase A after oral administration. Proc Natl Acad Sci U S A 1999;96:13989–94.

21. Wang H, Nan L, Yu D, Lindsey JR, Agrawal S, Zhang R. Anti-tumor efficacy of a novel antisense anti-mdm2 mixed-backbone oligonucleotide in human colon cancer models: p53-dependent and p53-independent mechanisms. Mol Med 2002;8:185–99.

22. Wang H, Yu D, Agrawal S, Zhang R. Experimental therapy of human prostate cancer by inhibiting MDM2 expression with novel mixed-backbone antisense oligonucleotides: *in vitro* and *in vivo* activities and mechanisms. Prostate 2003;54:194–205.

23. Zhang Z, Li M, Wang H, Agrawal S, Zhang R. Antisense therapy targeting MDM2 oncogene in prostate cancer: effects on proliferation, apoptosis, multiple gene expression, and chemotherapy. Proc Natl Acad Sci U S A 2003;100:11636–41.

24. Cummings J, Ward TH, LaCasse E, et al. Validation of pharmacodynamic assays to evaluate the clinical efficacy of an antisense compound (AEG 35156) targeted to the X-linked inhibitor of apoptosis protein XIAP. Br J Cancer 2005;92:532–8.

25. Kandimalla ER, Bhagat L, Wang D, et al. Divergent synthetic nucleotide motif recognition pattern: design and development of potent immunomodulatory oligodeoxyribonucleotide agents with distinct cytokine induction profiles. Nucleic Acids Res 2003;31:2393–400.

26. Fulda S, Wick W, Weller M, Debatin KM. Smac agonists sensitize for Apo2L/TRAIL- or anticancer drug-induced apoptosis and induce regression of malignant glioma *in vivo*. Nat Med 2002;8:808–15.

27. Ng CP, Bonavida B. X-linked inhibitor of apoptosis (XIAP) blocks Apo2 ligand/tumor necrosis factor-related apoptosis-inducing ligand-mediated apoptosis of prostate cancer cells in the presence of mitochondrial activation: sensitization by overexpression of second mitochondria-derived activator of caspase/direct IAP-binding protein with low pI (Smac/DIABLO). Mol Cancer Ther 2002;1:1051–8.

28. Guo F, Nimmanapalli R, Paranawithana S, et al. Ectopic overexpression of second mitochondria-derived activator of caspases (Smac/DIABLO) or cotreatment with N-terminus of Smac/DIABLO peptide potentiates epothilone B derivative- (BMS 247550) and Apo-2L/TRAIL-induced apoptosis. Blood 2002;99:3419–26.

29. Leaman DW, Chawla-Sarkar M, Vyas K, et al. Identification of X-linked inhibitor of apoptosis-associated factor-1 as an interferon-stimulated gene that augments TRAIL Apo2L-induced apoptosis. J Biol Chem 2002;277:28504–11.

30. McManus DC, Lefebvre CA, Cherton-Horvat G, et al. Loss of XIAP protein expression by RNAi and antisense approaches sensitizes cancer cells to functionally diverse chemotherapeutics. Oncogene 2004;23:8105–17.

31. Cummins JM, Kohli M, Rago C, Kinzler KW, Vogelstein B, Bunz F. X-linked inhibitor of apoptosis protein (XIAP) is a nonredundant modulator of tumor necrosis factor-related apoptosis-inducing ligand (TRAIL)-mediated apoptosis in human cancer cells. Cancer Res 2004;64:3006–8.

32. Li L, Thomas RM, Suzuki H, De Brabander JK, Wang X, Harran PG. A small molecule Smac mimic potentiates TRAIL- and TNFα-mediated cell death. Science 2004;305:1471–4.

33. Yamaguchi Y, Shiraki K, Fuke H, et al. Targeting of X-linked inhibitor of apoptosis protein or survivin by short interfering RNAs sensitize hepatoma cells to TNF-related apoptosis-inducing ligand- and chemotherapeutic agent-induced cell death. Oncol Rep 2005;14:1311–6.

34. Lowe SW, Cepero E, Evan G. Intrinsic tumour suppression. Nature 2004;432:307–15.

35. Igney FH, Krammer PH. Death and anti-death: tumour resistance to apoptosis. Nat Rev Cancer 2002;2:277–88.

36. Tong QS, Zheng LD, Wang L, et al. Downregulation of XIAP expression induces apoptosis and enhances chemotherapeutic sensitivity in human gastric cancer cells. Cancer Gene Ther 2005;12:509–14.

37. Yang X, Xing H, Gao Q, et al. Regulation of HtrA2/Omi by X-linked inhibitor of apoptosis protein in chemoresistance in human ovarian cancer cells. Gynecol Oncol 2005;97:413–21.

38. Hu P, Han Z, Couvillon AD, Exton JH. Critical role of endogenous Akt/IAPs and MEK1/ERK pathways in counteracting endoplasmic reticulum stress-induced cell death. J Biol Chem 2004;279:49420–9.

39. Pardo OE, Lesay A, Arcaro A, et al. Fibroblast growth factor 2-mediated translational control of IAPs blocks mitochondrial release of Smac/DIABLO and apoptosis in small cell lung cancer cells. Mol Cell Biol 2003;23:7600–10.

40. Chawla-Sarkar M, Bae SI, Reu FJ, Jacobs BS, Lindner DJ, Borden EC. Downregulation of Bcl-2, FLIP or IAPs (XIAP and survivin) by siRNAs sensitizes resistant melanoma cells to Apo2L/TRAIL-induced apoptosis. Cell Death Differ 2004;30:1–9.

41. Berezovskaya O, Schimmer AD, Glinskii AB, et al. Increased expression of apoptosis inhibitor protein XIAP contributes to anoikis resistance of circulating human prostate cancer metastasis precursor cells. Cancer Res 2005;65:2378–86.

42. Kaur S, Wang F, Venkatraman M, Arsura M. X-linked inhibitor of apoptosis (XIAP) inhibits c-Jun N-terminal kinase 1 (JNK1) activation by transforming growth factor β1 (TGF-β1) through ubiquitin-mediated proteosomal degradation of the TGF-β1-activated kinase 1 (TAK1). J Biol Chem 2005;280:38599–608.

43. Lima RT, Martins LM, Guimaraes JE, Sambade C, Vasconcelos MH. Specific downregulation of bcl-2 and xIAP by RNAi enhances the effects of chemotherapeutic agents in MCF-7 human breast cancer cells. Cancer Gene Ther 2004;11:309–16.

44. Liu Z, Li H, Derouet M, et al. ras oncogene triggers up-regulation of cIAP2 and XIAP in intestinal epithelial cells: epidermal growth factor receptor-dependent and -independent mechanisms of ras-induced transformation. J Biol Chem 2005;280:37383–92.

45. Hatano M, Mizuno M, Yoshida J. Enhancement of C2-ceramide antitumor activity by small interfering RNA on X chromosome-linked inhibitor of apoptosis protein in resistant human glioma cells. J Neurosurg 2004;101:119–27.

46. Marienfeld C, Yamagiwa Y, Ueno Y, et al. Translational regulation of XIAP expression and cell survival during hypoxia in human cholangiocarcinoma. Gastroenterology 2004;127:1787–97.

47. Mohapatra S, Chu B, Zhao X, Pledger WJ. Accumulation of p53 and reductions in XIAP abundance promote the apoptosis of prostate cancer cells. Cancer Res 2005;65:7717–23.

48. Cao C, Mu Y, Hallahan DE, Lu B. XIAP and survivin as therapeutic targets for radiation sensitization in preclinical models of lung cancer. Oncogene 2004;23:7047–52.

49. Carter BZ, Milella M, Tsao T, et al. Regulation and targeting of antiapoptotic XIAP in acute myeloid leukemia. Leukemia 2003;17:2081–9.

50. Miranda MB, Dyer KF, Grandis JR, Johnson DE. Differential activation of apoptosis regulatory pathways during monocytic vs granulocytic differentiation: a requirement for Bcl-X(L) and XIAP in the prolonged survival of monocytic cells. Leukemia 2003;17:390–400.

51. Hu Y, Cherton-Horvat G, Dragowska V, et al. Antisense oligonucleotides targeting XIAP induce apoptosis and enhance therapeutic activity against human lung cancer cells when combined with anticancer drug *in vitro* and *in vivo*. Clin Cancer Res 2003;9:2826–36.

52. Trauzold A, Schmiedel S, Roder C, et al. Multiple and synergistic deregulations of apoptosis-controlling genes in pancreatic carcinoma cells. Br J Cancer 2003;89:1714–21.

53. Roa WH, Chen H, Fulton D, et al. X-linked inhibitor regulating TRAIL-induced apoptosis in chemoresistant human primary glioblastoma cells. Clin Invest Med 2003;26:231–42.

54. Ravi R, Fuchs EJ, Jain A, et al. Resistance of cancers to immunologic cytotoxicity and adoptive immunotherapy via X-linked inhibitor of apoptosis protein expression and coexisting defects in mitochondrial death signaling. Cancer Res 2006;66:1730–9.

55. Park SJ, Wu CH, Gordon JD, Zhong X, Emami A, Safa AR. Taxol induces caspase-10-dependent apoptosis. J Biol Chem 2004;279:51057–67.

56. Nicklin PL, Bayley D, Giddings J, et al. Pulmonary bioavailability of a phosphorothioate oligonucleotide (CGP 64128A): comparison with other delivery routes. Pharm Res 1998;15:583–91.

57. Vidal L, Blagden S, Attard G, de Bono J. Making sense of antisense. Eur J Cancer 2005;41:2812–8.

Clinical Cancer Research

Preclinical Characterization of AEG35156/GEM 640, a Second-Generation Antisense Oligonucleotide Targeting X-Linked Inhibitor of Apoptosis

Eric C. LaCasse, Gabriele G. Cherton-Horvat, Kimberley E. Hewitt, et al.

Clin Cancer Res 2006;12:5231-5241.